



Publication Year	2016
Acceptance in OA	2020-06-25T13:47:10Z
Title	3C 279 IN OUTBURST IN 2015 JUNE: A BROADBAND SED STUDY BASED ON THE INTEGRAL DETECTION
Authors	BOTTACINI, EUGENIO, Böttcher, Markus, PIAN, Elena, Collmar, Werner
Publisher's version (DOI)	10.3847/0004-637X/832/1/17
Handle	http://hdl.handle.net/20.500.12386/26209
Journal	THE ASTROPHYSICAL JOURNAL
Volume	832



3C 279 IN OUTBURST IN 2015 JUNE: A BROADBAND SED STUDY BASED ON THE *INTEGRAL* DETECTION

EUGENIO BOTTACINI^{1,2}, MARKUS BÖTTCHER³, ELENA PIAN^{4,5,6}, AND WERNER COLLMAR⁷

¹W.W. Hansen Experimental Physics Laboratory & Kavli Institute for Particle Astrophysics and Cosmology,
Stanford University, USA; eugenio.bottacini@stanford.edu

²Dipartimento di Fisica e Astronomia “G. Galilei”, Università di Padova, I-35131 Padova, Italy

³Centre for Space Research, North-West University, Potchefstroom 2531, South Africa

⁴INAF, Istituto di Astrofisica Spaziale e Fisica Cosmica, via P. Gobetti 101, I-40129 Bologna, Italy

⁵Scuola Normale Superiore, Piazza dei Cavalieri 7, I-56122 Pisa Italy

⁶INFN, Sezione di Pisa, Largo Pontecorvo 3, I-56127 Pisa, Italy

⁷Max-Planck-Institut für extraterrestrische Physik, Giessenbach, D-85748 Garching, Germany

Received 2016 April 14; revised 2016 September 9; accepted 2016 September 12; published 2016 November 11

ABSTRACT

Blazars radiate from radio through gamma-ray frequencies and thereby make ideal targets for multifrequency studies. Such studies allow the properties of the emitting jet to be constrained. 3C 279 is among the most notable blazars and therefore subject to extensive multifrequency campaigns. We report the results of a campaign ranging from near-IR to gamma-ray energies that targeted an outburst of 3C 279 in 2015 June. The campaign pivots around the detection in only 50 ks by *INTEGRAL*, whose IBIS/ISGRI data pin down the high-energy component of the spectral energy distribution (SED) between *Swift*-XRT data and *Fermi*-LAT data. The overall SED from near-IR to gamma rays can be well represented by either a leptonic or a lepto-hadronic radiation transfer model. Even though the data are equally well represented by the two models, their inferred parameters challenge the physical conditions in the jet. In fact, the leptonic model requires parameters with a magnetic field far below equipartition with the relativistic particle energy density. In contrast, equipartition may be achieved with the lepto-hadronic model, although this implies an extreme total jet power close to the Eddington luminosity.

Key words: accretion, accretion disks – galaxies: individual (3C 279) – galaxies: jets – radiation mechanisms: non-thermal – X-rays: galaxies

1. INTRODUCTION

Blazars are radio-loud, jet-dominated active galactic nuclei (AGNs) with their jets closely aligned with the line of sight to the observer. Due to this geometric arrangement, their emission is strongly Doppler-enhanced. Consequently, they are bright sources from radio wavelengths to gamma-ray energies and allow for detailed multifrequency studies. Precise modeling of the multiwavelength emission allows us to constrain the physical properties of the emitting source. However, the emission from blazars is known to be variable on various timescales (Aharonian et al. 2007; Albert et al. 2007). Therefore, for a meaningful interpretation of these properties and emission mechanisms, the observations need to be at least quasi-simultaneous and to cover a wide range of frequencies. Such a detailed multifrequency campaign was carried out on the prominent blazar 3C 279. The campaign pivots around its detection by the *INTEGRAL* mission during an outburst in 2015 June. This outburst exhibited the source’s brightest flare ever observed at GeV energies (Cutini 2015; Lucarelli et al. 2015; Paliya 2015). 3C 279, at redshift $z = 0.5362$ (Marziani et al. 1996), is among the most luminous and variable extragalactic objects and gained prominence due to its bright flaring state detected by the Energetic Gamma Ray Experiment Telescope at the beginning of the *Compton Gamma-Ray Observatory*’s mission (Hartman et al. 1992), and it was the first (of currently only five) flat-spectrum radio quasar detected by ground-based atmospheric Cerenkov telescope facilities in very-high-energy (VHE: $E > 100$ GeV) gamma rays (Albert et al. 2008; Mirzoyan 2015). An interesting finding regarding 3C 279 is the change in the optical polarization angle following a gamma-

ray flare (Abdo et al. 2010) that was seen also in a number of other blazars, as shown in a recent study by Kiehlmann et al. (2016). Therefore, this intriguing source is subject to extensive monitoring programs revealing low-activity and high-activity states. In a low-activity state, the modeling of the broadband spectral energy distribution (SED) at X-ray energies is quite satisfactory (e.g., Collmar et al. 2010), while in some cases in a high-activity state of the source the same modeling is challenging (e.g., Hayashida et al. 2015).

In this work, we report the detection in the hard X-ray band of an outburst of 3C 279 around which a multifrequency campaign is centered. First, we detail the multifrequency campaign, followed by the compilation of the broadband SED and its modeling.

2. OBSERVATIONS AND DATA ANALYSES OF 3C 279

2.1. X-Ray Observations

INTEGRAL—A monitoring campaign on 3C 279 was performed by the *INTEGRAL* mission during its extragalactic survey program on the Coma sky area. While surveying the sky, astrophysical sources are monitored by *INTEGRAL*’s instruments because of their wide field of view (FOV). This approach of monitoring has provided excellent opportunities for single-source studies (e.g., Bottacini et al. 2010). During the Coma survey observations in 2015 June, *INTEGRAL* detected 3C 279 (Bottacini et al. 2015) with its imager IBIS (Ubertini et al. 2003) using the ISGRI detector (Lebrun et al. 2003). This is IBIS’s low-energy detector sensitive to photons of 15–1000 keV and having a FOV of 29×29 deg². IBIS/ISGRI

Table 1
3C 279: Hard X-Ray and X-Ray Spectral Fits

Observation (Inst. obs. id)	Start (date UTC)	Exposure (s)	Model	Γ	Norm	Chi-square	dof	Flux (10^{-11} erg cm^{-2} s^{-1})
IBIS 12200240002	2015 Jun 15 15:46:00	50000	pegpwlw	$1.08_{0.15}^{1.98}$	$1.62_{1.09}^{2.16}$	4.79	5	$7.83_{3.57}^{10.45}$
XRT 00035019176	2015 Jun 15 14:27:58	1995	abs*powerlaw	$1.37_{1.30}^{1.44}$	$5.84_{5.48}^{6.20}$	32.22	35	$2.27_{2.19}^{2.37}$
XRT 00092194008	2015 May 26 09:20:59	1115	abs*powerlaw	$1.85_{1.71}^{1.99}$	$3.35_{2.99}^{3.69}$	14.33	19	$0.703_{0.640}^{0.705}$

Note. Normalization: IBIS/ISGRI in units of 10^{10} erg cm^{-2} s^{-1} in the 20–100 keV band; *Swift*-XRT in units of 10^{-3} photons keV^{-1} cm^{-2} s^{-1} . Fluxes: IBIS/ISGRI flux is given in the 18–55 keV band; *Swift*-XRT flux is computed in the 2–6 keV band. Errors are reported at 1σ level.

data from this observation are analyzed with the latest version 10.2 of the standard Off-line Scientific Analysis software⁸ provided by the *INTEGRAL* Science Data Centre (Courvoisier et al. 2003) using the method described in Bottacini et al. (2012). With this software we analyze the *INTEGRAL* data set of revolution 1553 that comprised 15 Science Windows, each of which corresponds to a ~ 3500 s pointed observation. These add up to a total exposure time of ~ 50 ks. Only one Science Window (155300040010) has a much shorter exposure of ~ 500 s. The quality of this single observation is comparable to all the other Science Windows. The id numbers of the analyzed Science Windows run from 155300040010 (2015 June 15 15:46 UTC) to 155300170020 (2015 June 16 05:13 UTC) and account for pointed observations only. In the resulting mosaic sky image, thanks to its wide FOV, IBIS/ISGRI is able to detect 3C 279 even at a far off-axis angle (14°) with respect to the center of the dither pattern at 5.7σ in the energy range 18–55 keV at a constant flux level. The source spectrum in the energy range 20–100 keV can be fit with a flux-pegged power-law model `pegpwlw` of XSPEC (Arnaud 1996), which allows for normalization by total flux, with a spectral index of $1.08_{0.15}^{1.98}$. The result is reported in Table 1. A timing analysis of this *INTEGRAL* observation shows a rather constant flux displayed in the light curve of Figure 1. Unfortunately, because the center of the dither pattern of this *INTEGRAL* survey on the Coma region is at a large angular distance from 3C 279, the smaller FOV of JEM-X and OMC did not allow for an observational coverage of the source at X-ray and optical frequencies, respectively. Moreover, we have analyzed IBIS/ISGRI data of *INTEGRAL* revolution 1545 including Science Windows from 154500300010 (2015 May 26 04:16 UTC) to 154500470010 (2015 May 26 23:13 UTC), which did not yield a detection of 3C 279. However, the non-detection is used in the discussion in Section 4.

Swift-XRT—During the *INTEGRAL* monitoring of 3C 279, the source was observed nearly simultaneously by *Swift*-XRT in photon counting mode on 2015 June 15 14:27 UTC (obs id: 00035019176). The observation log is reported in Table 1. Data analysis is performed using `xrtproducts` and HEASoft 6.17. In agreement with the very timely analysis by Pittori et al. (2015a), we find the spectrum to be affected by pile-up. To correct for this effect we extract the spectrum from an annular region (rather than from a circular region) that excludes the central circular area of 2 pixels radius. The outer radius of the annulus is 30 pixels and the background is extracted from a source-free circular region of 50 pixels (each pixel corresponds to $\sim 2''36$, Moretti et al. 2004). The background spectrum accounts for less than 1% of the total net count rate. We generated the ancillary response file with `xrtmkarf` and we

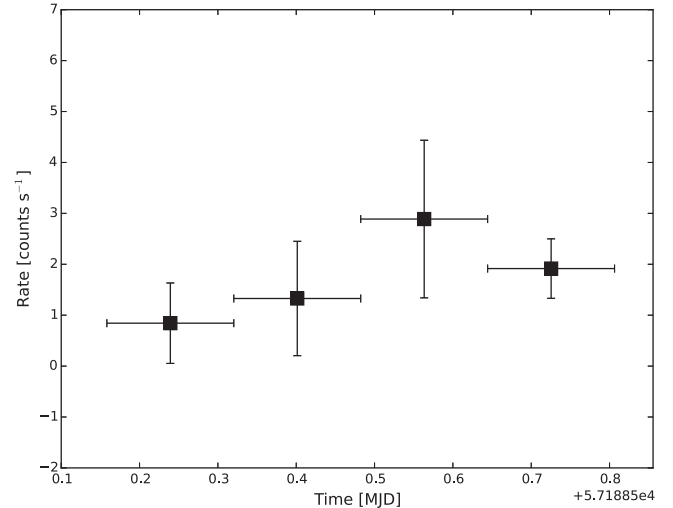


Figure 1. IBIS/ISGRI light curve of 3C 279 binned to 12.5 ks.

used the response matrix of `swxpc0to12s6_20130101v014.rmf`⁹ To confidently use the chi-square statistic for spectral fitting, we bin the data to at least 20 counts bin^{-1} . The spectrum is fitted in the energy range 0.6–6.0 keV. The baseline fit model is a power law with neutral hydrogen absorption (`wabs*powerlaw`) fixed to the Galactic value, which is $N_{\text{H}}^{\text{gal}} = 2.2 \times 10^{20}$ atoms cm^{-2} obtained from the LAB Survey of Galactic H I database (Kalberla et al. 2005). We do not find any evidence for excess absorption or for more sophisticated models. The fit results and derived values, which are in agreement with the analysis by Pittori et al. (2015a), are reported in Table 1. No significant variability within this observation is found (see the light curve in Figure 2). Additionally, we have analyzed *Swift*-XRT observation 00092194008 (2015 May 26 09:20 UTC), which is used in the discussion in Section 4.

2.2. UV to Near-IR Observations

Swift-UVOT—Simultaneously with the *INTEGRAL* and *Swift*-XRT observations, the UV–Optical Telescope (UVOT, Roming et al. 2005) on board the *Swift* satellite observed 3C 279 with its filter of the day, which was the *U* filter. We use the standard pipeline products, which are co-added and corrected for exposure. The standard $5'$ aperture is used for photometry. The resulting magnitude is $U = 14.92 (\pm 0.03)$, which is in agreement with the detailed analysis in Pittori et al.

⁸ <http://www.isdc.unige.ch/integral/analysis#Software>

⁹ <http://heasarc.gsfc.nasa.gov/docs/heasarc/caldb/data/swift/xrt/index.html>

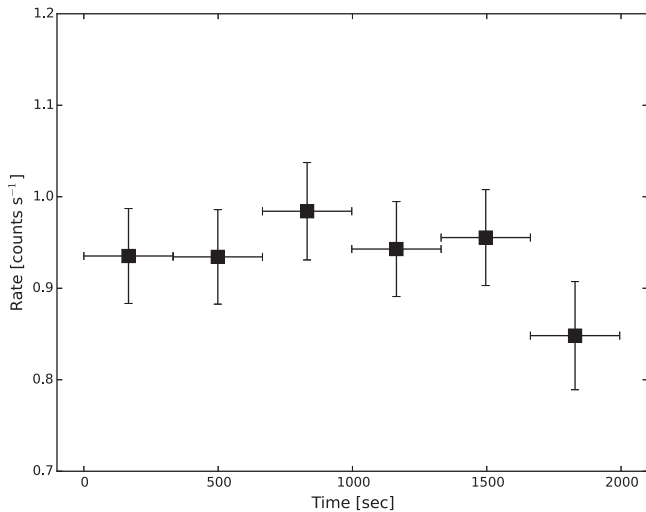


Figure 2. *Swift*-XRT light curve of 3C 279 binned to ~ 300 s.

(2015b). To convert magnitudes to fluxes we use the constants of the photometric system in Poole et al. (2008).

SMARTS—The blazar 3C 279 is part of an extensive monitoring program run by Yale University with the Small and Moderate Aperture Research Telescope System (SMARTS). During the *INTEGRAL* monitoring, SMARTS has been monitoring the source quasi-simultaneously. Data reduction and analysis are detailed in Bonning et al. (2012). Observations are performed in the optical and near-IR bands *B*, *V*, *R*, *J*, and *K* (see Table 2). Similarly to a precise study by Larionov et al. (2008), we convert magnitudes to fluxes using the constants from Mead et al. (1990).

Correction for the effect of interstellar extinction of data collected by *Swift*-UVOT and SMARTS is presented in Section 3.

2.3. Gamma-ray Observations

Simultaneously with the *INTEGRAL* observations, 3C 279 was also observed at MeV and GeV gamma-ray energies. The detection by the Italian *AGILE* mission (Tavani et al. 2008) is detailed in Lucarelli et al. (2015), and the *Fermi* gamma-ray mission has detected 3C 279 (Cutini 2015) simultaneously with *INTEGRAL* at GeV energies with its Large Area Telescope (LAT; Atwood et al. 2009). A prompt analysis of this detection of 3C 279 was performed in a precise time-resolved spectral study by Paliya (2015). From this study, we take the LAT spectral results for the time window that is contemporaneous with the IBIS/ISGRI observations and that shows resolved variability on a 6 hr timescale.

3. SED AND ITS MODELING

Even though the line of sight to the source is hardly affected by extinction because of its position at high Galactic latitude, we correct for this attenuation in the near-IR, optical, and UV bands (i.e., SMARTS and UVOT data). We compute the extinction with Cardelli’s law (Cardelli et al. 1989) with a reddening coefficient of $R_V = 3.1$ and an extinction coefficient in the *V* band of $A_V = 0.095$ (Schlegel et al. 1998).

The SED of 3C 279 displays the two broad non-thermal radiation components characteristic of blazars. The low-energy component is well understood as being due to synchrotron

Table 2
UV to Near-IR Observations

Instrument	Start (UTC)	Filter	Mag.	Mag. Error
SMARTS	2015 Jun 15 23:15:24	<i>B</i>	15.706	0.004
SMARTS	2015 Jun 15 23:19:21	<i>V</i>	15.187	0.004
SMARTS	2015 Jun 15 23:22:24	<i>R</i>	14.662	0.004
SMARTS	2015 Jun 15 23:15:20	<i>J</i>	12.903	0.005
SMARTS	2015 Jun 15 23:19:18	<i>K</i>	10.651	0.003
UVOT	2015 Jun 15 14:32:11	<i>U</i>	14.92	0.03

emission by relativistic electrons (possibly also positrons) in the jet, while the high-energy component can be either due to Compton scattering by the same relativistic electrons (leptonic processes) or due to proton-synchrotron radiation and synchrotron emission from secondaries produced in photo-pion interactions (hadronic processes). The peak position of the high-energy component is well constrained by the LAT data: the best-fit log-parabola spectrum having a spectral index $\alpha = 2.05 (\pm 0.05)$ indicates that the peak of the SED is at $\nu_{\text{HE}} \lesssim 3 \times 10^{22}$ Hz (Paliya 2015). The onset of the high-energy component is constrained by the *Swift*-XRT data. The onset and the peak of the high-energy component are bridged by the IBIS/ISGRI data. At low energies, the synchrotron component is constrained by the *Swift*-UVOT and SMARTS data, placing its peak at frequencies below $\nu_{\text{sy}} \lesssim 10^{14}$ Hz.

To model the overall SED, we adopt the two complementary approaches mentioned above: a leptonic and a hadronic model. Their time-independent homogeneous one-zone jet radiation transfer is used as described in detail in Böttcher et al. (2013), building upon the earlier work of Böttcher et al. (1997) and Böttcher & Chiang (2002). In both models, a spherical (in the comoving frame) emission region of radius R moves with bulk Lorentz factor Γ (corresponding to a speed of $\beta_{\Gamma}c$) within an angle θ_{obs} that determines the Doppler factor $\delta = (\Gamma [1 - \beta_{\Gamma} \cos \theta_{\text{obs}}])^{-1}$. The emitting volume is pervaded by a randomly oriented magnetic field of strength B and it is subject to injection of relativistic leptons (and protons, in the case of a hadronic model) with a comoving power-law distribution in particle energies ($i = e, p$ for electrons/positrons and protons, respectively):

$$Q_i^{\text{inj}}(\gamma; t) = Q_{i,0}^{\text{inj}}(t) \gamma_i^{-q} \text{ [cm}^{-3} \text{ s}^{-1}] \text{ for } \gamma_{i,1} \leq \gamma_i \leq \gamma_{i,2}, \quad (1)$$

which may be thought of as the result of an unspecified, rapid acceleration mechanism, such as first-order Fermi acceleration at a shock traveling through the jet.

In the leptonic model, the electron cooling is driven by synchrotron and inverse-Compton emission. For the latter the code accounts for synchrotron self-Compton (SSC) and external radiation fields from the accretion disk (EC-disk) known to be present in this source (e.g., Pian et al. 1999; Hartman et al. 2001) and an isotropic external radiation field, which represents the emission from the broad-line region (BLR—EC-BLR) or an infrared-emitting dust torus (EC-DT). A detailed description can be found in Böttcher et al. (2013). The solution for the equilibrium state between particle injection, cooling, and escape from the spherical volume is self-consistently computed. The result is illustrated by the red solid curve in Figure 3, and the model parameters are reported in Table 3. In this model, the *Swift*-XRT X-ray emission is

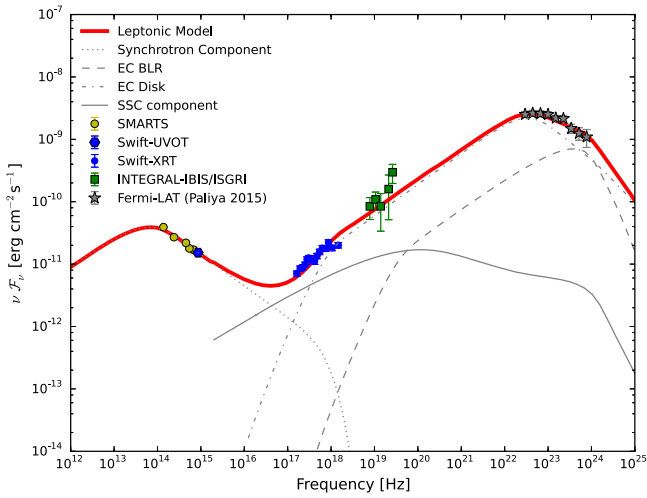


Figure 3. Quasi-simultaneous SED of 3C 279, along with the leptonic (red solid) model, as described in the text. In the leptonic model, the different line styles represent the individual emission components: synchrotron (dotted), synchrotron self-Compton (solid), external Compton scattering of accretion disk photons (dotted-dashed), external Compton scattering of BLR radiation (dashed), and the sum of all components (solid). See Table 3 for model parameters.

produced by a combination of SSC and EC-disk emission. The observational evidence for the existence of this latter component in the X-ray regime of 3C 279 has been set forth in an early multifrequency study of 3C 279 by Pian et al. (1999). Even though in that work the source was in a low-activity state, the same EC-disk component alone might dominate the hard X-ray emission in the *INTEGRAL* regime. The *Fermi*-LAT spectrum is a combination of the EC-disk radiation dominating at lower energies and the EC-BLR emission dominating above a few GeV. The slope of the injected electron distribution of 3 can plausibly be obtained, e.g., in diffuse shock acceleration at oblique relativistic shocks (e.g., Summerlin & Baring 2012). The photon energy densities due to the accretion disk and of the isotropic external radiation field in the stationary rest frame of the AGN are 4.9 erg cm^{-3} and $3.0 \times 10^{-3} \text{ erg cm}^{-3}$, respectively. The inferred location of the emitting region is 0.011 pc from the supermassive black hole. The resulting power in Poynting flux obtained from a magnetic field $B = 1 \text{ G}$ is $L_B = 2.0 \times 10^{44} \text{ erg s}^{-1}$ and the kinetic power carried in relativistic electrons is $L_e = 2.1 \times 10^{45} \text{ erg s}^{-1}$. This corresponds to a magnetization parameter of $\epsilon_B \equiv L_B/L_e = 0.095$, indicating that the emission region is dominated by kinetic energy by a factor of ~ 10 . These modeling results are underpinned by the observationally well constrained accretion disk and BLR parameters.

In the lepto-hadronic model, in addition to the leptonic processes described above, the contribution of ultrarelativistic protons to the radiative output is accounted for. The protons are subject to synchrotron radiation and photo-pion production. As hadronic models require significantly higher magnetic fields (typically of order $\sim 100 \text{ G}$) than leptonic ones, electron cooling is strongly dominated by synchrotron emission, and the dominant target photon field for photo-pion production by the relativistic protons is the comoving synchrotron radiation of the primary electrons with a photon energy density $u'_{\text{syn}} = 2.5 \times 10^{-2} \text{ erg cm}^{-3}$, which can be compared with the energy density of the magnetic field, $u'_B = 570 \text{ erg cm}^{-3}$. The assumed dominance of the synchrotron emission over the

external radiation photon field places the emitting region necessarily outside the BLR to satisfy the requirement of $u'_{\text{syn}} > \Gamma^2 \times u_{\text{ext}}$. The equilibrium particle (electron/positron and proton) spectra and the radiative outputs are calculated self-consistently, as described in Böttcher et al. (2013). The result is shown by the green solid curve in Figure 4, and the model parameters are listed in Table 3. In the lepto-hadronic model, the entire X-ray through gamma-ray emission is strongly dominated by proton-synchrotron radiation, with a negligible contribution from photo-pion-induced processes. The model requires a magnetic field of $B = 100 \text{ G}$, corresponding to a power carried in Poynting flux of $L_B = 1.5 \times 10^{48} \text{ erg s}^{-1}$, compared with a power carried in relativistic protons of $L_p = 1.6 \times 10^{48} \text{ erg s}^{-1}$ and in relativistic leptons of $L_e = 1.9 \times 10^{42} \text{ erg s}^{-1}$. It is obvious that the kinetic energy in the jet is strongly dominated by the relativistic protons, and the magnetization parameter, i.e., the ratio of magnetic-field energy to kinetic energy carried in the jet, is $\epsilon_B \approx L_B/L_p = 0.9$. This indicates that in this model, kinetic and magnetic energy are significantly closer to equipartition than in the case of our leptonic model. Additionally, for the external radiation field to be negligible, the emission region has to be located outside the BLR, which will also allow for potential VHE gamma-ray emission to escape unattenuated. Figures 3 and 4 illustrate that both (leptonic and lepto-hadronic) models are able to almost indistinguishably represent the SED data, and both models are able to reproduce the spectral curvature seen in the *Fermi*-LAT gamma-ray spectrum well. However, the lepto-hadronic model requires a very hard spectral index of the proton spectrum of 1.8, which may be difficult to realize in nature. It is furthermore subject to the well-known extreme power requirements of lepto-hadronic models of blazars (e.g., Böttcher et al. 2013; Diltz et al. 2015; Petropoulou & Dimitrakoudis 2015), which may be incompatible with our current understanding of jet launching mechanisms (Zdziarski & Böttcher 2015). Specifically, our model requires a total jet power of $L_{\text{jet}} \approx 3.1 \times 10^{48} \text{ erg s}^{-1}$, which is almost exactly equal to the Eddington luminosity of the $2.5 \times 10^8 M_{\odot}$ black hole powering the AGN in 3C 279. This finding regarding the total jet power is strengthened by the equipartition condition known to be close to the minimal energy requirement.

4. DISCUSSION

The active state of 3C 279 in 2015 June allowed for a 5.7σ detection with IBIS/ISGRI in only $\sim 50 \text{ ks}$ of observations. This can be compared with a quiescent state, in which IBIS/ISGRI needs an exposure ~ 10 times longer ($\sim 500 \text{ ks}$) for a 7.5σ detection as shown in a multifrequency study by Collmar et al. (2010). To explore possible hard X-ray variability on longer timescales, we analyzed the data of *INTEGRAL* revolution 1545 a month earlier, in 2015 May, for a total exposure of $\sim 44 \text{ ks}$. This did not yield a detection, which indicates that the source was in a quiescent state. A confirmation of this finding is provided by a simultaneous *Swift*-XRT observation (id 00092194008, see Table 1) that reveals the source flux to be three times lower than in the active state. This draws a consistent picture of the source state: it indicates that the hard X-ray emission of 3C 279 is variable, and that this variability may be correlated with the soft X-ray variability, as expected in both model scenarios considered here, in which the emission in both frequency regimes is produced by the same relativistic particle population. We find

Table 3
List of Parameters from SED Modeling

Model (1)	R (2)	η_{esc} (3)	B (4)	Γ (5)	γ_{min} (6)	γ_{max} (7)	q (8)	γ_{pmin} (9)	γ_{pmax} (10)	q_{p} (11)
Leptonic	1	7	1	20	1×10^3	1×10^5	3
Lepto-hadronic	1	1	100	20	1×10^2	1×10^4	3	1×10^3	6×10^8	1.8

Note. Explanation of columns: (1) SED model; (2) radius of emitting volume $\times 10^{16}$ cm; (3) escape time parameter: $t_{\text{esc}} = \eta_{\text{esc}} \times R/c$; (4) magnetic field in gauss; (5) bulk Lorentz factor; (6) and (7) minimum and maximum random Lorentz factors of injected electrons; (8) slope of the injected electron distribution; (9) and (10) low- and high-energy cut-offs of the proton spectrum in GeV; (11) slope of the injected proton distribution.

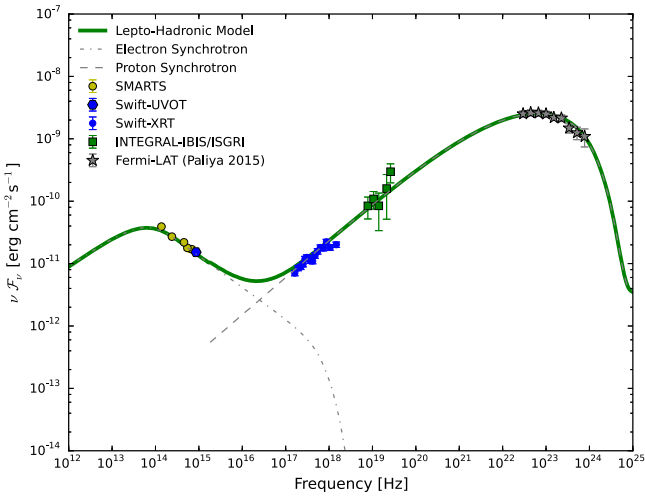


Figure 4. Quasi-simultaneous SED of 3C 279, along with the lepto-hadronic (green solid) model, as described in the text. In the lepto-hadronic model, the different components are: primary electron synchrotron (dotted-dashed) and proton synchrotron (dashed). See Table 3 for model parameters.

that homogeneous, single-zone radiation transfer models provide a satisfactory representation of the SED, in both a leptonic and a lepto-hadronic scenario.

Our leptonic SED model indicates that the emission region needs to be dominated by kinetic energy by a factor of ~ 10 with respect to the energy carried in magnetic fields. Such a situation may be difficult to realize in scenarios of jet formation and acceleration in which the magnetic field is the primary source of jet power, because one would naturally expect any mechanism that converts magnetic-field energy to particle kinetic energy to cease once approximate equipartition is reached. A particle acceleration scenario involving relativistic shocks in a particle-dominated jet (e.g., Marscher & Gear 1985; Sokolov et al. 2004; Joshi & Böttcher 2011) and/or shear layer acceleration in a spine-sheath geometry (e.g., Stawarz & Ostrowski 2002; Ghisellini et al. 2005) may provide a suitable alternative. In the leptonic scenario the inferred location of the emitting region is well within the BLR (at 0.011 pc from the supermassive black hole), so VHE photons would not be able to escape this region unattenuated (Böttcher & Els 2016). Thus, our model predicts that no VHE emission should have been detected from this flare, if not originating at a different location. Such a location is found to be far beyond the BLR of 3C 279 in order for VHE photons of ~ 100 GeV to be detectable, as derived in a dedicated study of the gamma-ray emission site by Dermer et al. (2014). In fact, the single highest-energy gamma-ray revealed by the *Fermi*-LAT in this flare from 3C 279 is detected at no more than ~ 52 GeV (Paliya 2015).

In contrast, our lepto-hadronic SED model allows us to choose parameters close to equipartition between the magnetic field and the relativistic proton population. This model requires a spectral index for proton injection of 1.8, which is harder than what one would expect, e.g., in standard scenarios of particle acceleration at non-relativistic shocks or relativistic, parallel shocks. However, diffusive shock acceleration at relativistic, oblique shocks (Summerlin & Baring 2012) or at relativistic shear layers (e.g., Rieger & Duffy 2006) may produce relativistic particle spectra much harder than E^{-2} . Further support for the lepto-hadronic scenario is provided by the quite good agreement in terms of the minimum-time variability of ~ 6.2 hr derived from our modeling and the measured resolved variability of ~ 6 hr in the study of Paliya (2015). In our modeling, we have assumed that the comoving electron-synchrotron radiation field dominates over external radiation fields, which requires the emission region to be located outside the BLR. An important issue for the lepto-hadronic model may be the extreme jet power, of the order of the Eddington luminosity of the central black hole in 3C 279. Our observations show that *INTEGRAL* data tie in with both the *Swift*-XRT soft X-ray data and the *Fermi*-LAT gamma-ray data, forming a straight power law, which strongly suggests that it is one single emission component that is responsible for the entire X-ray through gamma-ray spectrum. This is compatible with the proton-synchrotron interpretation.

The low-energy synchrotron emission and the high-energy inverse-Compton emission originate in the very same region under the assumption of one-zone radiation transfer. With this assumption, the leptonic model cannot explain the observed low-energy and high-energy variability in many cases (e.g., Böttcher et al. 2009; Nalewajko et al. 2012; Paliya et al. 2016), which calls for alternative sophisticated models including the lepto-hadronic model, although that faces the issue of the extreme jet power in our study. Dedicated studies of hadronic processes are also put forward in a sophisticated work by Ackermann et al. (2016) to explain sub-orbital scale variability in two out of 11 one-orbit bins during a *Fermi*-LAT ‘Target of Opportunity’ observation. A time-dependent lepto-hadronic model (e.g., Diltz et al. 2015) might represent a viable avenue for a solution.

In quiescent states of 3C 279, leptonic models can often reproduce the SED satisfactorily (e.g., Collmar et al. 2010; Zheng & Yang 2016). Such modeling suggests that the gamma-ray emission site is outside the BLR (Zheng & Yang 2016) and thus makes the detection of VHE photons possible. On the other hand, the leptonic model is far from equipartition (Böttcher et al. 2009) when trying to reproduce the VHE data from the Major Atmospheric Gamma-ray Imaging Cerenkov (MAGIC) telescope (Albert et al. 2008). However, those data

can be well explained in the context of a lepto-hadronic model (Böttcher et al. 2009).

5. CONCLUSIONS

3C 279 was caught in outburst by *INTEGRAL*–*IBIS*/*ISGRI* in 2015 June. The multifrequency campaign around this detection has collected observations in the optical, X-ray, hard X-ray, and gamma-ray bands. The SED of these observations can be equally well modeled by a leptonic model and by a lepto-hadronic one. Yet, the derived parameters of these models challenge the physical conditions in the jet. In fact, for the leptonic model it is not possible to obtain an arrangement that is even approximate to equipartition. The same model also predicts that no VHE photons should have been detected during this outburst. In contrast, an arrangement close to equipartition in the lepto-hadronic scenario favors this model, even though the jet power remains extreme. Our *INTEGRAL* data tie in with *Swift*-*XRT* and *Fermi*-*LAT* data and form a straight power law, which is compatible with the proton-synchrotron component of the lepto-hadronic scenario.

We thank the anonymous referee for an exhaustive and constructive refereeing process. We also thank the *INTEGRAL* and *Swift* teams for the observations. This research is based on observations with *INTEGRAL*, an ESA project with instruments and science data center funded by ESA member states (especially the PI countries: Denmark, France, Germany, Italy, Switzerland, Spain) and Poland, and with the participation of Russia and the USA. This paper has made use of up-to-date SMARTS optical/near-infrared light curves that are available at www.astro.yale.edu/smarts/glast/home.php. This research has made use of the NASA/IPAC Extragalactic Database (NED), which is operated by the Jet Propulsion Laboratory, of data obtained from the High Energy Astrophysics Science Archive Research Center (HEASARC) provided by NASA’s Goddard Space Flight Center. E.P. acknowledges partial support from the Italian Ministry for Research and Scuola Normale Superiore, and grants ASI INAF I/088/06/0, INAF PRIN 2011, and PRIN MIUR 2010/2011. The work of M.B. is supported by the South African Research Chair Initiative (SARChI) of the Department of Science and Technology and the National Research Foundation¹⁰ of South Africa through SARChI Chair grant No. 64789. E.B. acknowledges support through NASA grants NNX13AO84G, NNX13AF13G, and partial support through grant NNX16AF27G. This paper is dedicated in memory of Lea Bottacini.

Facilities: *Fermi*, *INTEGRAL*, *Swift*, SMARTS.

REFERENCES

- Abdo, A. A., Ackermann, M., Ajello, M., et al. 2010, *Natur*, 463, 919
 Ackermann, M., Anantua, R., Asano, K., et al. 2016, *ApJL*, 824, L20
 Aharonian, F., Akhperjanian, A. G., Bazer-Bachi, A. R., et al. 2007, *ApJL*, 664, L71
 Albert, J., Aliu, E., Anderhub, H., et al. 2007, *ApJ*, 669, 862
 Albert, J., Aliu, E., Anderhub, H., et al. 2008, *Sci*, 320, 1752
 Arnaud, K. A. 1996, *adass*, 101, 17
 Atwood, W. B., Abdo, A. A., Ackermann, M., et al. 2009, *ApJ*, 697, 1071
 Bonning, E., Urry, C. M., Bailyn, C., et al. 2012, *ApJ*, 756, 13
 Bottacini, E., Ajello, M., & Greiner, J. 2012, *ApJS*, 201, 34
 Bottacini, E., Böttcher, M., Schady, P., et al. 2010, *ApJL*, 719, L162
 Bottacini, E., Ferrigno, C., Fotopoulou, S., et al. 2015, *ATel*, 7648
 Böttcher, M., & Chiang, J. 2002, *ApJ*, 581, 127
 Böttcher, M., & Els, P. 2016, *ApJ*, 821, 102
 Böttcher, M., Mause, H., & Schlickeiser, R. 1997, *A&A*, 324, 395
 Böttcher, M., Reimer, A., & Marscher, A. P. 2009, *ApJ*, 703, 1168
 Böttcher, M., Reimer, A., Sweeney, K., & Prakash, A. 2013, *ApJ*, 768, 54
 Cardelli, J. A., Clayton, G. C., & Mathis, J. S. 1989, *ApJ*, 345, 245
 Collmar, W., Böttcher, M., Krichbaum, T. P., et al. 2010, *A&A*, 522, A66
 Courvoisier, T. J.-L., Walter, R., Beckmann, V., et al. 2003, *A&A*, 411, L53
 Cutini, S. 2015, *ATel*, 7633
 Dermer, C. D., Cerruti, M., Lott, B., Boisson, C., & Zech, A. 2014, *ApJ*, 782, 82
 Diltz, C. D., Böttcher, M., & Fossati, G. 2015, *ApJ*, 802, 133
 Ghisellini, G., Tavecchio, F., & Chiaberge, M. 2005, *A&A*, 432, 401
 Hartman, R. C., Bertsch, D. L., Fichtel, C. E., et al. 1992, *ApJL*, 385, L1
 Hartman, R. C., Böttcher, M., Aldering, G., et al. 2001, *ApJ*, 553, 683
 Hayashida, M., Nalewajko, K., Madejski, G. M., et al. 2015, *ApJ*, 807, 79
 Joshi, M., & Böttcher, M. 2011, *ApJ*, 727, 21
 Kalberla, P. M. W., Burton, W. B., Hartmann, D., et al. 2005, *A&A*, 440, 775
 Kiehlmann, S., Savolainen, T., Jorstad, S. G., et al. 2016, *A&A*, 590, A10
 Larionov, V. M., Jorstad, S. G., Marscher, A. P., et al. 2008, *A&A*, 492, 389
 Lebrun, F., Leray, J. P., Lavocat, P., et al. 2003, *A&A*, 411, L141
 Lucarelli, F., Pittori, C., Verrecchia, F., et al. 2015, *ATel*, 7631
 Marscher, A. P., & Gear, W. K. 1985, *ApJ*, 298, 114
 Marziani, P., Sulentic, J. W., Dultzin-Hacyan, D., Calvani, M., & Moles, M. 1996, *ApJS*, 104, 37
 Mead, A. R. G., Ballard, K. R., Brand, P. W. J. L., et al. 1990, *A&AS*, 83, 183
 Mirzoyan, R. 2015, *ATel*, 7080
 Moretti, A., Campana, S., Tagliaferri, G., et al. 2004, *Proc. SPIE*, 5165, 232
 Nalewajko, K., Sikora, M., Madejski, G. M., et al. 2012, *ApJ*, 760, 69
 Paliya, V. S. 2015, *ApJL*, 808, L48
 Paliya, V. S., Diltz, C., Böttcher, M., Stalin, C. S., & Buckley, D. 2016, *ApJ*, 817, 61
 Petropoulou, M., & Dimitrakoudis, S. 2015, *MNRAS*, 452, 1303
 Pian, E., Urry, C. M., Maraschi, L., et al. 1999, *ApJ*, 521, 112
 Pittori, C., Verrecchia, F., Puccetti, S., et al. 2015a, *ATel*, 7639
 Pittori, C., Verrecchia, F., Puccetti, S., et al. 2015b, *ATel*, 7668
 Poole, T. S., Breeveld, A. A., Page, M. J., et al. 2008, *MNRAS*, 383, 627
 Rieger, F., & Duffy, P. 2006, *ApJ*, 652, 1044
 Roming, P. W. A., Kennedy, T. E., Mason, K. O., et al. 2005, *SSRv*, 120, 95
 Schlegel, D. J., Finkbeiner, D. P., & Davis, M. 1998, *ApJ*, 500, 525
 Sokolov, A., Marscher, A. P., & McHardy, I. M. 2004, *ApJ*, 613, 725
 Stawarz, L., & Ostrowski, M. 2002, *ApJ*, 578, 763
 Summerlin, E. J., & Baring, M. G. 2012, *ApJ*, 745, 63
 Tavani, M., Barbiellini, G., Argan, A., et al. 2008, *NIMPA*, 588, 52
 Ubertini, P., Lebrun, F., Di Cocco, G., et al. 2003, *A&A*, 411, L131
 Zdziarski, A. A., & Böttcher, M. 2015, *MNRAS*, 450, L21
 Zheng, Y. G., & Yang, C. Y. 2016, *MNRAS*, 457, 3535

¹⁰ Any opinion, finding, and conclusion or recommendation expressed in this material is that of the authors and the NRF does not accept any liability in this regard.